Dynamics and Disorder in Surfactant-Templated Silicate Layers Studied by Solid-State NMR Dephasing Times and Correlated Line Shapes

Sylvian Cadars,[‡] Nicolas Mifsud, Anne Lesage, Jan Dirk Epping,[†,§] Niklas Hedin,[†,||] Bradley F. Chmelka,[†] and Lyndon Emsley*

Laboratoire de Chimie (UMR 5182 CNRS/ENS Lyon), Ecole Normale Supérieure de Lyon, 46 allée d'Italie, 69364 Lyon cedex 07, France

Received: December 03, 2007; Revised Manuscript Received: March 17, 2008

Surfactant-templated layered silicates are shown to possess complex compositional, structural, and dynamic features that manifest rich and interrelated order and disorder at molecular length scales. Temperature-dependent 1D and 2D solid-state ^{29}Si NMR measurements reveal a chemical-exchange process involving the surfactant headgroups that is concomitant with reversible broadening of ^{29}Si NMR line shapes under magic-angle-spinning (MAS) conditions at temperatures in the range 205−330 K. Specifically, the temperature-dependent changes in the ^{29}Si transverse dephasing times T_2' can be quantitatively accounted for by 2-fold reorientational dynamics of the surfactant headgroups. Variable-temperature analyses demonstrate that the temperature-dependent ^{29}Si shifts, peak broadening, and 2D ^{29}Si{^{29}Si} correlation NMR line shapes are directly related to the freezing of the surfactant headgroup dynamics, which results in local structural disorder within the silicate framework.

1. Introduction

Mesostructured and mesoporous inorganic solids have specific properties that make them attractive for a wide range of potential applications in catalysis,[1] separations,[2] or optoelectronics.[3,4] The properties of these solids depend on their compositions, structures, and dynamics, often across several length scales, which are challenging to characterize, understand, and control.[5,6] Solid-state nuclear magnetic resonance (NMR) spectroscopy plays a crucial role in the characterization of these materials at a molecular level, complementing other methods, such as X-ray diffraction, electron microscopy, and bulk property measurements (see ref 7 for a recent review). Notably, solid-state NMR can provide quantitative and/or correlated molecular information on crystalline or amorphous organic or inorganic solids (see, for example, refs 8–13) and is therefore especially useful for the characterization of heterogeneous systems with different extents of order and disorder, including inorganic−organic hybrid materials. New state-of-the-art NMR methodologies can provide crucial information on local compositions, structures, interactions, and dynamics, along with insights on their distributions within complicated heterogeneous materials.

Recently, surfactant-templated layered silicates with high degrees of short-range order have been synthesized and characterized,[14,15] with analyses indicating subtle and rich extents of disorder, the origins of which have remained unknown. Two-dimensional (2D) ^{29}Si{^{29}Si} magic-angle-spinning (MAS) NMR experiments[15] have shown that the ^{29}Si resonances in these systems are inhomogeneously broadened, due to the presence of slight structural disorder at different four-coordinated ^{29}Si sites in the silicate framework. In particular, a wide range of elongated 2D line shapes have been observed that are characteristic of inhomogeneous distributions of isotropic chemical shifts arising from local correlated disorder.[15–17] This disorder may originate in several different ways with distinctly different ramifications with respect to the local structure. For example, the chemical shift distribution could be induced, on one hand, by a dispersion in the arrangements of the ionically interacting surfactant headgroups with respect to the silicate layers or, on the other hand, by slight deviations of the covalent bonding geometry in the silicate layers. Detailed understanding of slight disorder presents a major challenge to solid-state NMR and to materials characterization in general, and has, so far, received far less attention than characterization of highly disordered systems, such as glasses, or highly ordered materials, such as crystalline solids.

Here, we characterize the slight disorder in an inorganic−organic hybrid solid with both highly ordered and highly disordered domains that are intimately mixed, and with large areas of interfacial contact. Specifically, we examine surfactant-templated layered silicates, which present heterogeneous structures and dynamics involving both the inorganic and organic components. Local structures within the silicate layers are examined by variable-temperature solid-state 2D ^{29}Si MAS NMR and coherence-dephasing-time analyses, which show that the disorder is directly related to the surfactant headgroup dynamics.

Notably, we demonstrate that ^{29}Si NMR transverse dephasing times can be used to measure dynamic processes independently of static disorder, which can be examined separately by variable-temperature ^{29}Si MAS NMR line shape analyses. Specifically, temperature-dependent changes in the ^{29}Si transverse dephasing times T_2' allow quantitative characterization of the reorientational dynamics of the surfactant headgroups. The reversible broadening of the ^{29}Si NMR spectra at low temper-

* Corresponding author. Phone: +33 4 72 72 84 86. Fax: +33 4 72 72 88 60. E-mail: lyndon.emsley@ens-lyon.fr.

† Department of Chemical Engineering, University of California, Santa Barbara, CA 93106.

‡ Present address: Department of Chemical Engineering, University of California, Santa Barbara, CA 93106.

§ Present address: Institut für Chemie, Fachgruppe Anorganische und Analytische Chemie, Technische Universität Berlin, Berlin, Germany.

|| Present address: Materials Chemistry Research Group, Department of Physical, Inorganic and Structural Chemistry, Arrhenius Laboratory, Stockholm University, SE 106 91 Stockholm, Sweden.

10.1021/jp711398h CCC: $40.75
Published on Web 05/29/2008

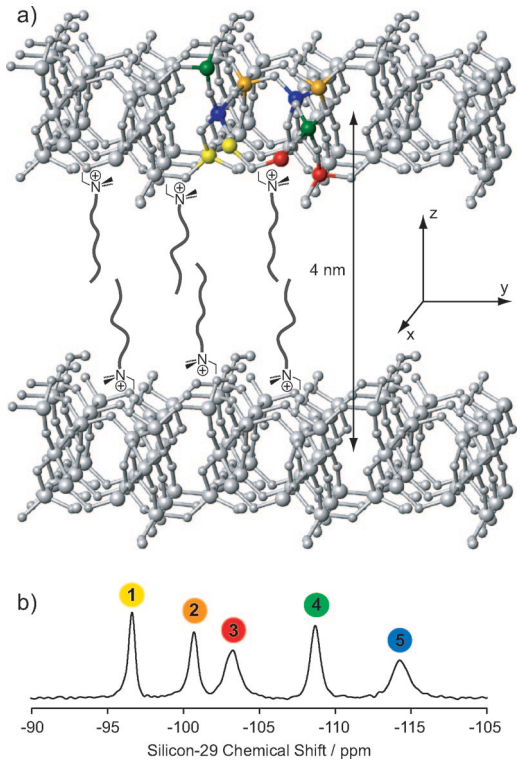

Figure 1. (a) Schematic diagram of the molecularly ordered silicate layers and templating $CH_3(CH_2)_{15}Me_2EtN^+$ surfactant molecules. The structure of the silicate layers and color code labels for the different ^{29}Si sites are the same as in ref 15. (b) The 99.4 MHz $^{29}Si\{^1H\}$ CP-MAS spectrum of a powder sample of the surfactant-templated silicate layers recorded at 298 K, which shows the five equally populated crystallographically distinct ^{29}Si sites.

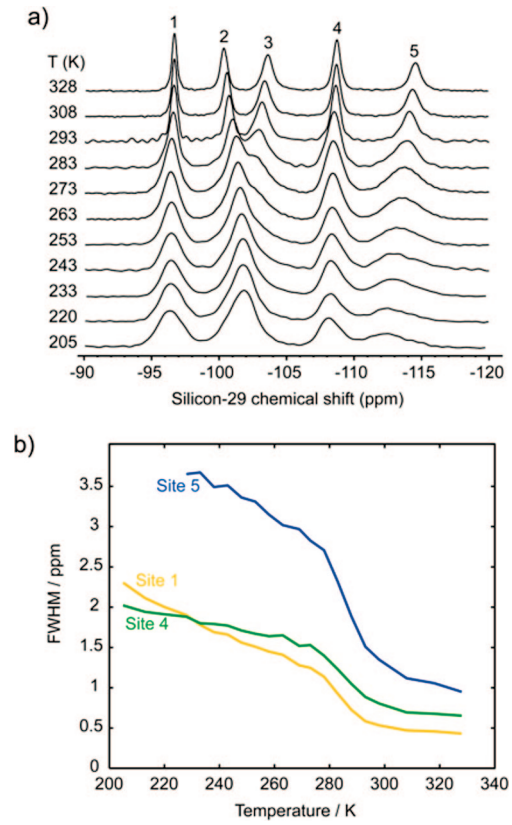

Figure 2. (a) Temperature-dependent ^{29}Si CP-MAS NMR spectra of the surfactant-templated 50% ^{29}Si-enriched layered silicate indicated in Figure 1. Both broadening and shifts in the ^{29}Si peak positions are observed with decreasing temperature. (b) Plots of the full-width-at-half-maximum (fwhm) line width Δ^* as a function of temperature for the three ^{29}Si sites that remain resolved over the whole temperature range of 205–330 K considered here. The yellow, green, and blue curves correspond to sites 1, 4, and 5, respectively.

atures is attributed to reversible changes in local order within the silicate layers, concomitant with changes in surfactant mobility. The ^{29}Si nuclei are *spectators* of the headgroup dynamics, reported through their T_2', and *actors* in reporting their own dynamically modulated local disorder, through their chemical shifts. Because these two effects can be observed at the same time and independently, they can be clearly distinguished. Combined analyses of temperature-dependent isotropic ^{29}Si chemical shifts, ^{29}Si peak broadening, and 2D $^{29}Si-^{29}Si$ chemical shift correlations between pairs of sites establish that these manifestations result from a single physical process that is intrinsically related to the freezing of the surfactant headgroup dynamics.

2. NMR Line Shape Analyses

Self-assembled layered silicate−surfactant materials with high degrees of short-range structural order have been prepared with 50% ^{29}Si-enrichment in the silicate framework, using $CH_3(CH_2)_{15}N^+(Me_2Et)$ surfactant molecules as structure-directing species (where "Et" and "Me" represent ethyl and methyl groups, respectively).[14,15] The three-dimensional (3D) structure of the inorganic framework proposed in ref 15, which is consistent with combined multidimensional $^{29}Si\{^{29}Si\}$ NMR, X-ray crystallography, and density functional theory results, is shown in Figure 1a, together with a schematic representation of the alkylammonium surfactant species. Colored silicon atoms correspond to the five inequivalent four-coordinated ^{29}Si sites labeled 1, 2, 3, 4, and 5 (with the same color code as in ref 15) as resolved in the one-dimensional (1D) $^{29}Si\{^1H\}$ cross-polarization magic-angle-spinning (CP-MAS) NMR spectrum shown in Figure 1b. These include three distinct ^{29}Si sites with peaks at −103, −108, and −114 ppm that correspond to fully condensed Q^4 moieties, as well as peaks at −97 and −101 ppm, corresponding to Q^3 moieties. The incompletely condensed Q^3 sites interact with the structure-directing cationic surfactant headgroups or with protons as silanol species.[15] Electrostatic interactions between cationic structure-directing species and anionic Q^3 silicate sites influence strongly the development of molecular order in the framework.[14,18]

A reversible ordering/disordering process within the silicate framework is observed through temperature-dependent changes in the 1D and 2D ^{29}Si MAS NMR spectra. In the following, analyses of 1D and 2D $^{29}Si\{^{29}Si\}$ NMR line shapes reveal that both inhomogeneous and homogeneous broadening are involved, which are associated with local structural disorder and dynamic processes, respectively. Figure 2a shows a series of $^{29}Si\{^1H\}$ CP-MAS spectra acquired at temperatures ranging from 205 (bottom) to 328 K (top), in which the resonances broaden and shift with sample cooling. The spectra recover their initial shapes when the temperature is increased back to room temperature. (The ^{29}Si signals associated with sites 2 and 3 overlap at low temperatures and are thus not studied in detail here.) In Figure 2b, the full-width-at-half-maximum (fwhm) values Δ^* of the ^{29}Si resonances associated with sites 1 (yellow), 4 (green), and 5 (blue) are plotted as functions of temperature, showing that the line widths do not vary linearly. Instead, an apparently critical regime is observed between 270 and 300 K, in which the line widths of all of the resolved ^{29}Si sites decrease dramatically with increasing temperature. This indicates that the

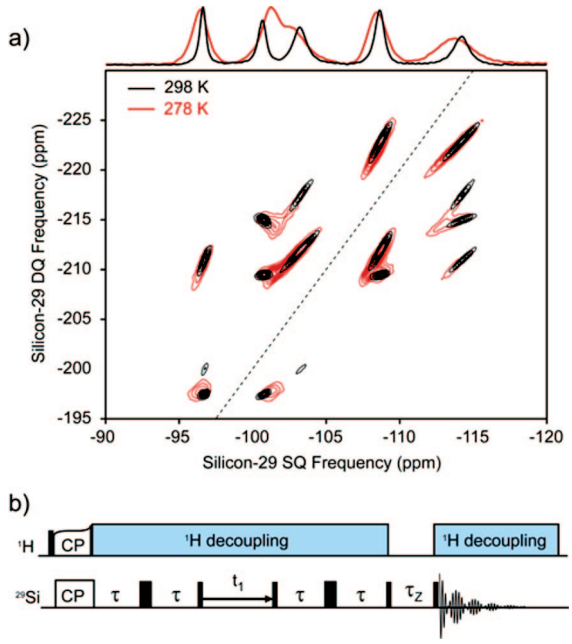

Figure 3. (a) Superposition of two $^{29}Si\{^{29}Si\}$ z-filtered refocused (zfr) INADEQUATE spectra acquired at 278 (red) and 298 K (black) under otherwise identical conditions for the surfactant-templated layered silicate (Figure 1). The different shapes and temperature dependences of the correlation peaks reveal the presence of a disordering process(es). In each spectrum, the contour levels correspond to 15, 25, 35, 45, 55, 65, 75, 85, and 95% of the maximum intensity. (b) Pulse sequence used to record the zrf-INADEQUATE spectra shown in (a). The z-filter allows elimination of undesired dispersive antiphase contributions due to multiple couplings.[21]

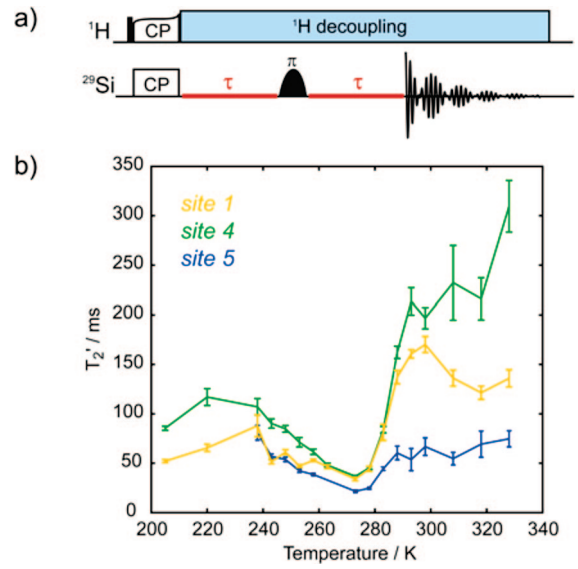

Figure 4. (a) Selective spin-echo pulse sequence for measuring transverse dephasing times T_2' in isotopically enriched solids. The use of a semiselective refocusing pulse allows for removal of J-coupling modulation. (b) Plots of the measured ^{29}Si T_2' values as functions of temperature for the ^{29}Si sites 1 (yellow), 4 (green), and 5 (blue) (Figure 1), which remain resolved over the 205−330 K temperature range considered. A critical temperature regime is observed around 275 K, where T_2' diminishes for each of the ^{29}Si sites.

temperature-dependent broadening of the different ^{29}Si signals shares a common origin for the different sites in the silicate layers.

The nature of this broadening can be characterized at a molecular level by 2D $^{29}Si\{^{29}Si\}$ NMR, which correlates interactions between different pairs of sites, including the development of temperature-dependent disorder. Figure 3a shows the superposition of two $^{29}Si\{^{29}Si\}$ z-filtered refocused (zfr) INADEQUATE[19–21] spectra for the same surfactant-templated layered silicate as in Figure 1, acquired at 298 K (in black) and 278 K (in red), using the pulse sequence shown in Figure 3b. Both spectra show a wide range of 2D line shapes arising from slight structural disorder of the various four-coordinate ^{29}Si sites in the silicate layers. The 2D ^{29}Si NMR line shapes are more elongated at low temperature, corresponding to an increased dispersion in the isotropic frequencies associated with a given site. Such *inhomogeneous* broadening of the 2D line shapes and the disorder that it reflects establish unambiguously what the 1D spectra could not, namely, that *the larger line widths arise due to broader distributions of local site environments*. Furthermore, a more detailed comparison of the line shapes also reveals small but significant broadening orthogonal to the main axes of the ellipsoidal peaks. This latter broadening is potentially of a different nature compared to the elongation of the peaks parallel to the main axes and could reflect a temperature-dependent *homogeneous* contribution. This type of broadening typically yields circular (as opposed to elliptical) line shapes in 2D correlation spectra, which are similar in effect to random variations in correlated signal intensities associated with different sites.[17] Broadening due to such homogeneous contributions can be probed directly by ^{29}Si transverse dephasing time measurements, which are based on spin echoes that refocus selectively the interactions that are responsible for the inhomogeneous broadening.

In the surfactant-templated layered silicate materials examined here, ^{29}Si transverse dephasing times appear to be significantly affected by a dynamic process or processes over the temperature range 240−300 K. It has recently been shown[16,17,19,22] that, for a given site, the refocused line width Δ', which is defined with respect to the transverse dephasing time T_2' during a spin echo, $\Delta' = (\pi T_2')^{-1}$, is usually much less than the apparent line width Δ^* in the 1D spectrum ($\Delta' \ll \Delta^*$). This is because the inhomogeneous broadening (Δ^*), due to a distribution of local environments (or bulk magnetic susceptibility), is entirely refocused by a rotor-synchronized spin echo, leaving only the nonrefocusable contributions to the line width (Δ'), such as residual dipolar couplings and relaxation effects. In particular, the nonrefocusable line width Δ' can be considered for disordered solids to be approximately the limiting homogeneous line width associated with a spin in a given local environment.[16,17] In protonated solids, Δ' is generally dominated by the residual heteronuclear dipolar couplings to the protons,[23,24] and therefore, measurements of transverse dephasing times T_2' have not, so far, been related to structural or dynamic parameters.

To evaluate the contribution of this nonrefocusable broadening to the 2D line shapes of the $^{29}Si\{^{29}Si\}$ zfr-INADEQUATE spectra shown in Figure 3a, systematic spin-echo measurements of transverse dephasing time T_2' of different ^{29}Si sites were conducted as a function of temperature. Partial ^{29}Si enrichment (ca. 50%) of the silicate framework enhanced signal sensitivity, but also the probability of $^{29}Si-O-^{29}Si$ pairs, leading to undesired (in the present case) $^2J(^{29}Si-O-^{29}Si)$-coupling modulations of the spin-echo intensity. Using the pulse sequence of Figure 4a, scalar couplings to the other spins are refocused by replacing the π pulse of the standard spin-echo experiment by a semiselective π pulse on the observed site.[25,26] In Figure 4b, the measured T_2' values are plotted for sites 1, 4, and 5 in yellow, green, and blue, respectively. A critical temperature regime is identified around 275 K, in which increased ^{29}Si transverse

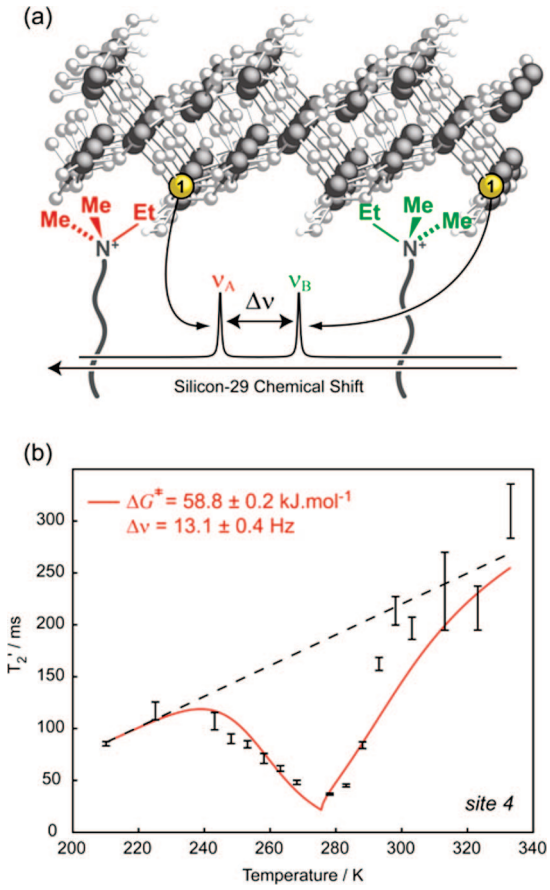

Figure 5. (a) Schematic diagram illustrating the postulated two-site model for describing the reorientational dynamics of the surfactant headgroups, and accompanying effects in the slow-exchange regime on the isotropic ^{29}Si chemical shift(s) for a given framework site. Coadsorbed water (or other solvent) molecules are expected to play a role in the process, but are omitted here for simplicity and clarity. (b) Plot of the measured ^{29}Si T_2' dephasing time values as a function of temperature for site 4 (Figure 1) in the layered silicate framework. The black dashed line corresponds to the phenomenological description of the residual dipolar and relaxation contributions to the transverse dephasing rate $T_2^0 = (R_2^{\text{ResDip}} + R_2^{\text{solid}})^{-1}$, best fit of the external points (T < 230 K and T > 295 K) to a linear temperature-dependence function. In red is shown the best fit of the central region (230 K < T < 295 K) to the liquid-state-like T_2^{exch} function described in the text, using the free energy of activation $\Delta G^{\ddagger}$ and the low-temperature splitting between the exchanging sites $\Delta\nu$ as optimized parameters.

dephasing is observed, corresponding to a broadening of the associated refocused line width Δ'. In the next section, we investigate the physical origins of the low T_2' values measured for all of the ^{29}Si sites in the layered silicate material near the critical temperature regime, ca. 275 K.

3. Chemical Exchange

Dynamic processes associated with temperature-dependent mobilities of the surfactant species over the temperature range 250−300 K can account principally for the observed T_2' measurements for the ^{29}Si sites. The variable-temperature ^{29}Si T_2' measurements were conducted under otherwise identical conditions (MAS and ^{1}H heteronuclear decoupling, in particular), to avoid introducing additional contributions to the T_2' behaviors from heteronuclear ^{29}Si−^{1}H dipolar couplings. This allows observation of common T_2' temperature minima for ^{29}Si sites 1, 4, and 5 near 280 K, as shown in Figure 4b, which thus appear to result from a dynamic process that is the dominant contribution to the ^{29}Si nonrefocusable broadening under these conditions.

The most likely candidates for the dynamics here are the surfactant species, whose mobilities will influence the nearby environments of the ^{29}Si sites in the layered silicate frameworks. The ^{29}Si nuclei can thus act as spectator probes of the local surfactant motions, which display strong temperature and also hydration dependencies. In particular, the reorientation dynamics of the surfactant headgroups can be quantified through the ^{29}Si T_2' measurements and then analyzed with respect to the disorder observed in the elongated 2D line shapes of ^{29}Si{^{29}Si} zfr-INADEQUATE spectra (Figure 3a). In general, a distribution of local environments may exist, due to the influence of several nearby surfactant headgroups on the local environment of a given ^{29}Si site, which contributes to the broadening of the ^{29}Si line shapes. Nevertheless, we show in the next section that a simple two-site chemical-exchange process (illustrated in Figure 5a) appears to account for the temperature-dependent dephasing times measured in Figure 4b. In the slow-exchange regime (i.e., at low temperatures), otherwise equivalent ^{29}Si sites within the silicate framework may experience subtly different chemical shifts, depending on the relative orientations of nearby asymmetric surfactant headgroups.

3.a. Basic Theory of Chemical Exchange in Liquid-State NMR. In liquid-state NMR, it is well-known that the transverse relaxation time T_2 can be used to obtain detailed information on molecular dynamics.[27,28] This is possible because of the dephasing that is induced by changes in the isotropic frequency of a given nucleus, due to chemical exchange on a time scale that is comparable to the reciprocal of the difference in chemical shifts associated with the exchanging sites. For the simplest case of exchange between two equally populated sites A and B in thermodynamic equilibrium

$$\text{A} \underset{k_{\text{exch}}}{\overset{k_{\text{exch}}}{\rightleftharpoons}} \text{B}$$

analytical formulas have been proposed that predict the transverse dephasing rate $R_2 = 1/T_2$ in the so-called intermediate-exchange regime in liquids:[29]

$$R_2 = R_2^{\text{liquid}} + R_2^{\text{exch}} \tag{1}$$

with

$$R_2^{\text{exch}} = k_{\text{exch}} - \sqrt{\frac{1}{2}(G + |G|)} \tag{2}$$

where $G = k_{\text{exch}}^2 - \pi^2\Delta\nu^2$; k_{exch} is the exchange rate, $\Delta\nu = |\nu_A - \nu_B|$ is the chemical shift difference in hertz between the isotropic frequencies of the observed sites A and B in the slow-exchange regime, and R_2^{liquid} is the liquid-state transverse relaxation rate in the absence of the chemical-exchange process. The exchange rate k_{exch} is related to the temperature by the Eyring equation:[30]

$$k_{\text{exch}} = \kappa \frac{k_B T}{h} \exp\left(-\frac{\Delta G^{\ddagger}}{RT}\right) \tag{3}$$

where $\Delta G^{\ddagger}$ is the free energy of activation, i.e., the energy difference between the transition state and the reactant, k_B is Boltzmann's constant, h is Planck's constant, R is the gas constant, and T is the absolute temperature. κ is the transmission coefficient that corresponds to the fraction of all reactant molecules that reach the transition state, and is taken equal to 1, as is generally the case for adiabatic reactions[31] (i.e., those proceeding without electronic transitions) with a single reaction path[32] ($\kappa = 1/n$ for an n-path reaction).[43]

3.b. T_2' as a Probe of Chemical Exchange in Solids. In solids, the situation is significantly different. The transverse dephasing rate $R_2' = 1/T_2'$ is, for spin-1/2 nuclei in protonated materials, dominated by the contribution from residual dipolar couplings R_2^{ResDip}. The incoherent (relaxation) contribution R_2^{solid} is generally expected to be much smaller than R_2^{ResDip} in the solid state, due to low molecular mobilities. We hypothesize that, in the critical exchange regime, R_2' may be dominated by the chemical-exchange contribution, R_2^{exch}, and thus have more liquid-like character. Consequently, R_2' can be modeled as follows:

$$R_2' = \frac{1}{T_2'} = R_2^{\mathrm{solid}} + R_2^{\mathrm{ResDip}} + R_2^{\mathrm{exch}} = \frac{1}{T_2^{\mathrm{solid}}} + \frac{1}{T_2^{\mathrm{ResDip}}} + \frac{1}{T_2^{\mathrm{exch}}} \tag{4}$$

with

$$R_2^{\mathrm{exch}} > R_2^{\mathrm{ResDip}} \gg R_2^{\mathrm{solid}} \tag{5}$$

in the intermediate-exchange regime. In such a case, the transverse dephasing time T_2' can be used to characterize quantitatively the chemical-exchange process, even in the presence of inhomogeneous broadening that obscures observation of the dynamics from the one-dimensional line shapes.

The ^{29}Si transverse dephasing behaviors presented above (Figure 4b) are analyzed within this model, where species A and B correspond to two distinct orientations of the surfactant headgroup near the considered ^{29}Si site (see Figure 5a), and which allows quantification of the dynamic process(es) involving the surfactant headgroups. For example, Figure 5b shows the measured ^{29}Si T_2' values of ^{29}Si site 4 in the layered silicate framework as a function of temperature. Outside the region near 270 K corresponding to the critical temperature, i.e. the intermediate-exchange regime in our hypothesis, T_2' is dominated by the complicated spin dynamics that are responsible for residual heteronuclear dipolar couplings that persist under conditions of incomplete heteronuclear decoupling and magic-angle spinning. This regime is described purely phenomenologically by fitting the points at $T < 240$ K and $T > 300$ K to a straight line:

$$T_2^0(T) = 1/\left(R_2^{\mathrm{solid}}(T) + R_2^{\mathrm{ResDip}}(T)\right) = aT + b \tag{6}$$

which is shown as a dashed line in Figure 5b.[44] $R_2^0(T) = 1/T_2^0$ is then inserted into the model represented by eq 4, with R_2^{exch} expressed as in eqs 2 and 3, and the experimental T_2' values are fitted to the resulting expression, with $\Delta G^{\ddagger}$ and $\Delta\nu$ as adjustable parameters. The corresponding best-fit and optimal values of $\Delta G^{\ddagger}$ and $\Delta\nu$ obtained for ^{29}Si site 4 are shown in red in Figure 5b. Our model is in very good agreement with the experimental data, and gives a free energy of activation $\Delta G^{\ddagger} = 58.8 \pm 0.2$ kJ·mol^{-1}, and low-temperature difference between pairs of ^{29}Si signals (albeit overlapping) $\Delta\nu = 13.1 \pm 0.4$ Hz[45] (i.e., 0.132 ± 0.004 ppm at 11.74 T), that are associated with the two orientations of the surfactant headgroup. Free energies of activation and low-temperature frequency differences of ^{29}Si signals have been obtained in the same way for ^{29}Si sites 1 and 5 from the measured T_2' values, and the results are summarized in Table 1. Interestingly, the calculated free energies of activation for the dynamic process at hand, as monitored by the temperature dependence of the T_2' values for the three ^{29}Si sites, are in excellent (and independent) agreement with each other. This corroborates the passive role of the ^{29}Si sites as spectators of a single dynamic process, which is attributed to the reorientation dynamics of the surfactant headgroups, whose direct characterization using ^{13}C, ^{1}H (see, for example, ref 18), or ^{2}H NMR is under current investigation in our groups.

TABLE 1: Free Energies of Activation of the Surfactant Headgroup Dynamics Measured from the T_2' Dephasing Time Values of ^{29}Si Sites 1, 4, and 5, and Associated Low-Temperature Frequency Differences $\Delta\nu = |\nu_A - \nu_B|$

^{29}Si Site	$\Delta G^{\ddagger}$ (kJ·mol^{-1})	$\Delta\nu$ (Hz)	$\Delta\nu$ (ppm)
1	58.6 ± 0.7	15 ± 15	0.15 ± 0.15
4	58.8 ± 0.2	13.1 ± 0.4	0.132 ± 0.004
5	58.8 ± 0.4	16 ± 1	0.16 ± 0.01

3.c. Chemical Exchange and Structural Disorder. The dynamic process of the surfactant headgroups described above accounts for the nonrefocusable broadening, but it does not directly account for the overall inhomogeneous broadening observed in the temperature dependence of the apparent line widths Δ^* (Figure 2b). Nevertheless, the inhomogeneous chemical shift distributions associated with the elongated two-dimensional line shapes and the effects due to chemical exchange can be analyzed in a concerted manner. The first question is whether the exchange dynamics measured through T_2' account for the observed line broadening at low temperatures. Figure 6a shows (black solid line) the static inhomogeneous distribution of ^{29}Si chemical shifts associated with site 4 estimated from the experimental ^{29}Si CP-MAS line shape at 310 K. This temperature corresponds to the fast-exchange regime of the surfactant species, and every individual position in the inhomogeneous distribution can thus be represented by a Lorentzian peak with an intrinsic ^{29}Si line width (fwhm) of $\Delta' = (\pi T_2')^{-1}$, where T_2' is the value measured at 310 K for site 4, as depicted for arbitrary positions by the blue, red, and yellow lines in Figure 6a. At lower temperatures, these individual lines

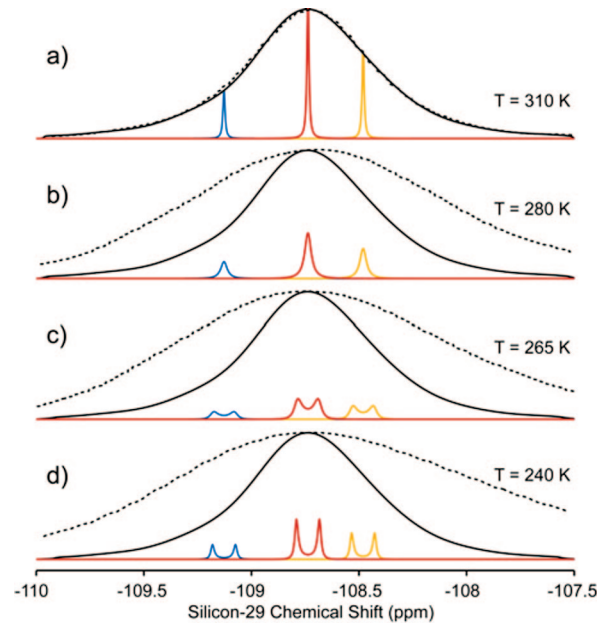

Figure 6. Plot of the expected temperature-dependent variations in the ^{29}Si NMR line shape of site 4 (Figure 2a), due to contributions associated with two-site exchange, to assess its role in accounting for the broadening of the ^{29}Si peaks. The blue, red, and yellow lines show the evolutions of individual lines calculated from the exchange process. The experimental lines at the corresponding temperatures (offset to match the position of the simulated maximum) are shown for comparison as dashed lines. Strong discrepancies between the predicted and experimental line shapes are attributed to the presence of a further disordering process concomitant with the surfactant headgroup reorientational dynamics.

are influenced by the chemical-exchange process determined in the previous section and broaden, as the intermediate-exchange regime is reached. This regime is defined by[33]

$$T_2^0 < \tau < \left(\frac{1}{2}\pi^2 \Delta\nu^2 T_2^0\right)^{-1} \quad (7)$$

where

$$\tau(T) = 1/k_{\mathrm{exch}}(T) = \frac{h}{\kappa k_B T} \exp\left(\frac{\Delta G^{\ddagger}}{RT}\right) \quad (8)$$

and $T_2^0(T)$, $\Delta\nu = \nu_B - \nu_A$, and $\Delta G^{\ddagger}$ are the same as discussed previously in section 3.b, and $\kappa = 1$. The shape $f_{\mathrm{exch}}(\nu)$ of the individual lines is then given by[33]

$$f_{\mathrm{exch}}(\nu) = \frac{2\tau(T)\Delta\nu^2}{(\nu - \nu_C)^2 + \pi^2\tau(T)^2(\nu - \nu_A)^2(\nu - \nu_B)^2} \quad (9)$$

where $\nu_C = (\nu_A + \nu_B)/2$. In analogy with liquid-state NMR, each individual line first broadens (Figure 6b) and then splits into two separately resolved broad lines (Figure 6c), which narrow as the temperature is reduced further (Figure 6d), until the slow-exchange regime is reached, and the line widths are no longer affected by temperature.

In Figure 6, we show several simulated predicted line shapes at different temperatures as solid black lines that include the effect of the exchange broadening described above, calculated across the entire broad chemical shift distribution. The experimentally observed line shapes at each temperature are shown as dashed lines (offset when required to match the maximum intensity of the simulated lines). While the experimental spectrum and the simulated line shape for two-site exchange agree at 310 K (Figure 6a), they deviate substantially at lower temperatures (Figure 6b−d)). From this, it is clear that the two-site jump of the surfactant headgroup characterized in section 3.b alone cannot be responsible for the increase of the apparent ^{29}Si line width Δ^* from 67 to 178 Hz fwhm observed for site 4 when the sample is cooled from 310 to 240 K. Therefore, another mechanism must also contribute to this broadening.[46] However, the critical variations in Δ^* observed for temperatures 270−300 K (Figure 2b) close to the intermediate-exchange regime of the surfactant headgroup rotation indicate that the additional disordering process is nevertheless related to (and possibly caused by) the freezing of the headgroup dynamics.

4. Nature of the Structural Disorder

The elongated 2D ^{29}Si{^{29}Si} double-quantum line shapes discussed above are thus attributed to unspecified static structural disorder, which is now discussed in light of the headgroup reorientation dynamics. Two-site ^{29}Si{^{29}Si} chemical shift correlations are compared with the temperature-dependent processes discussed previously, showing that they are probably of the same nature, specifically that the disordering process is (at least) concomitant with the freezing of the surfactant headgroup dynamics between 250 and 300 K. Such slowing of surfactant headgroup motions over this temperature range is expected to occur together with reduced mobility of coadsorbed water or other solvent species at the silicate layer surfaces, although these are difficult to characterize because of strong homonuclear ^{1}H dipole−dipole couplings. Information on the nature of the disordering process can nevertheless be extracted through cross-analyses of the correlated line shapes at 298 K (Figure 3, black spectrum) and the temperature dependence of the ^{29}Si chemical shifts in Figure 2a. To propose a quantitative analysis, we first examine the temperature-dependent shifts of the ^{29}Si MAS NMR peaks. The 2D ^{29}Si{^{29}Si} correlation line shapes, which are characteristic of the static structural disorder, are then analyzed by extraction of linear site-to-site chemical shift correlations, and the concept of "degree of chemical shift correlation" is introduced.

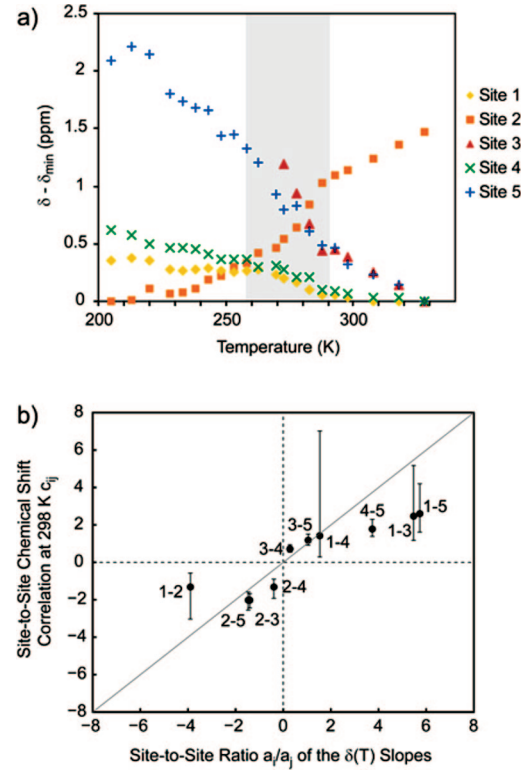

Figure 7. (a) Plot of the variation in the position of the maximum of each resolved peak in the series of ^{29}Si CP-MAS NMR spectra shown in Figure 2a as a function of temperature. Chemical shift values reported here are of the form $\delta_i(T) - \delta_{i,\mathrm{min}}$, with $i = 1, 2, \ldots, 5$ corresponding to the ^{29}Si site number and $\delta_{i,\mathrm{min}}$ to the minimum chemical shift value of site i over the temperature range 205−330 K. Site 1, 2, 3, 4, and 5 shifts are indicated by yellow diamonds (◆), orange squares (■), red triangles (▲), green crosses (×), and blue plus signs (+), respectively. (b) Correlation plot of the two-site chemical shift correlations c_{ji} between sites i and j ($i < j$), obtained from 2D ^{29}Si{^{29}Si} NMR spectra at 298 K, as a function of the ratios a_j/a_i ($i < j$) of the linear slopes associated with temperature-dependent chemical shift variations of sites i and j. The ranges indicated by the vertical bars are delimited by the slopes c_{ji}^1 and c_{ji}^2 extracted from CPM1 and CPM2 matrices (see section 4.b), and give an indication of the inverse of the degree of chemical shift correlation for the $i-j$ pair considered. The solid line is a guide to the eye that indicates the 1:1 axis.

4.a. Temperature-Dependent Shifts of ^{29}Si NMR Peaks. The temperature dependences of the 1D ^{29}Si MAS NMR peak positions over the range 205−330 K are illustrated in Figure 7a. For each ^{29}Si site i (ranging from 1 to 5), the chemical shift variations $\delta_i(T) - \delta_{i,\mathrm{min}}$ are shown as functions of temperature, where $\delta_i(T)$ is the position of the peak maximum at temperature T, and $\delta_{i,\mathrm{min}}$ is the lowest shift observed for site i in the temperature range of 205−330 K examined. This allows a comparison of the relative chemical shift changes of the different ^{29}Si sites as a function of temperature. As an estimate, these curves were fitted to linear functions of temperature, thus providing slopes a_i (in ppm/K) for each ^{29}Si site i, which are reported in Table 2. For each pair of sites $i-j$, the ratio of the corresponding slopes a_j/a_i is displayed in Table 2 using the convention $i < j$.

4.b. Static Disorder and Site-to-Site Chemical Shift Correlation Slopes. The static disorder within the silicate layers at 298 K is analyzed through site-to-site chemical shift correlation

TABLE 2: Measured Temperature-Dependent ^{29}Si Shift Slopes, Corresponding Site-to-Site Ratios, Experimental Site-to-Site Chemical Shift Correlations, and Degrees of Correlation

^{29}Si site (i)	$\delta(T)$ slopes a_i (ppm·K^{-1})	^{29}Si−^{29}Si pair	$\delta(T)$ slope ratio $(a_j/a_i)^a$	chemical shift correlation $(c_{ji})^b$	r_{ji}
1	−0.0035	1−2	−3.9	−1.32	0.44
2	0.014	1−3	5.5	2.47	0.48
3	−0.019	1−4	1.5	1.42[c]	0.20
4	−0.0053	1−5	5.7	2.60	0.62
5	−0.020	2−3	−1.4	−2.02[c]	0.82
		2−4	−0.4	−1.32	0.68
		2−5	−1.5	−2.01	0.79
		3−4	0.3	0.71	0.76
		3−5	1.0	1.17	0.78
		4−5	3.7	1.78	0.78

[a] With $i < j$. [b] With $i < j$. Extracted from the zfr-INADEQUATE spectrum at 298 K (Figure 3, black) according to the procedure described in section 4.b and Figure 8. [c] Slopes extracted from a post-C7 DQ spectrum at 298 K (Supporting Information, Figure S1) according to the procedure described in section 4.b.

slopes obtained for each ^{29}Si−^{29}Si pair using the following procedure. The 2D cross-peak spectral intensities were extracted from the ^{29}Si{^{29}Si} zfr-INADEQUATE spectrum of Figure 3(black) for *J*-coupled spin pairs, and a ^{29}Si{^{29}Si} post-C7 DQ NMR[34] spectrum (see Supporting Information, Figure S1) for the non-*J*-coupled pairs (i.e., sites 1−4 and 2−3). For each cross-peak two conditional probability matrices CPM1 and CPM2 were constructed as described in ref 17, and as summarized in Figure 8. A shearing transformation[35] is first applied to convert the DQ−SQ spectrum (Figure 8a) to a SQ−SQ spectrum (Figure 8b). Then, a SQ−SQ cross-peak associated with a given ^{29}Si−^{29}Si pair (e.g., sites 2−4 in Figure 8c) is extracted, whose columns or rows are normalized by making the sum of the intensities in either each column or each row equal to unity, respectively. (The "1" and "2" superscripts in the c^1_{ji} and c^2_{ji} variables are labels that refer to conditional probability matrices CPM1 and CPM2, respectively, from which they were extracted). This yields two conditional probability matrices CPM1 (Figure 8(d, left)) and CPM2 (Figure 8(d, right)). The intensity of a point CPM1(ω^i_4,ω^k_2) of the conditional probability distribution CPM1 yields the probability that ^{29}Si site 4 resonates at ω^i_4 given that ^{29}Si site 2 resonates at ω^k_2. Similarly, the intensity CPM2(ω^i_4,ω^k_2) of the conditional probability distribution CPM2 gives the probability that site 2 resonates at ω^k_2 given that site 4 resonates at ω^i_4.[17] The conditional probability distributions CPM1 and CPM2 thus only differ by the information that is considered known, namely the resonance frequency of site 2 or site 4, respectively.

Nearly all of the pairs show highly linear correlation profiles, as illustrated in Figure 9, indicating highly correlated local structural disorder within the silicate layers.[16,17] For each ^{29}Si−^{29}Si pair $i-j$ (ranging from 1 to 5, with $i < j$), correlation slopes c^1_{ji} and c^2_{ji} were extracted from matrices CPM1 and CPM2, respectively, by fitting the position of the maximum intensity of each row/column of CPM1 and CPM2 to straight lines (red lines in Figures 8d and 9). This gives the "orientation" of a given site-to-site ^{29}Si{^{29}Si} chemical shift correlation associated with its respective matrix. The differences observed between the correlation slopes c^1_{ji} and c^2_{ji} extracted from CPM1 and CPM2 for a specific ^{29}Si−^{29}Si pair indicate the degree of correlation between the chemical shifts of the two sites. The larger the difference is between c^1_{ji} and c^2_{ji}, the weaker the correlation is, up to the limit where CPM1 has a horizontal slope, and CPM2

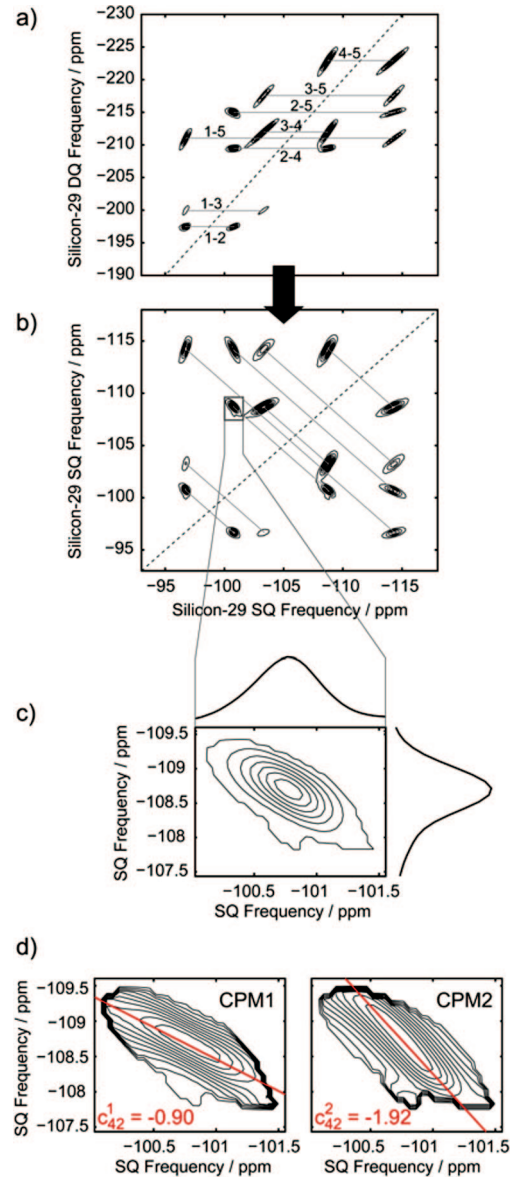

Figure 8. (a) A ^{29}Si{^{29}Si} zfr-INADEQUATE spectrum of the silicate layers (same as in Figure 3a (black)), with a lowest contour level of 8%. (b) SQ−SQ spectrum obtained by applying a shearing transformation to the zfr-INADEQUATE spectrum in (a). In this spectrum, pairs of cross-peaks are symmetric with respect to the diagonal. (c) Enlargement of the SQ−SQ cross-peak corresponding to the ^{29}Si−^{29}Si pair 2−4 outlined in (b). Above is shown the projection along the vertical axis, i.e., the 1D chemical shift distribution associated with site 2. On the right side is the chemical shift distribution of site 4, obtained from the projection of the selected cross-peak along the horizontal axis. (d) Conditional probability matrices CPM1 (d, left) and CPM2 (d, right) obtained by normalizing the columns and the rows, respectively, of the selected cross-peak in (c). Slopes c^1_{42} and c^2_{42} obtained from the best fit of the positions of maximum intensities of CPM1 and CPM2 to straight lines are shown as red solid lines in (d).

a vertical slope, which would indicate the absence of correlation. This can thus be quantified by first defining the overall chemical shift correlation c_{ji} between two ^{29}Si sites as the normalized geometric average of the two slopes:

$$c_{ji} = \frac{c^1_{ji}}{\left|c^1_{ji}\right|}\left(c^1_{ji}c^2_{ji}\right)^{1/2} \tag{10}$$

and the *degree of chemical shift correlation*, r_{ji}, is then determined as follows:

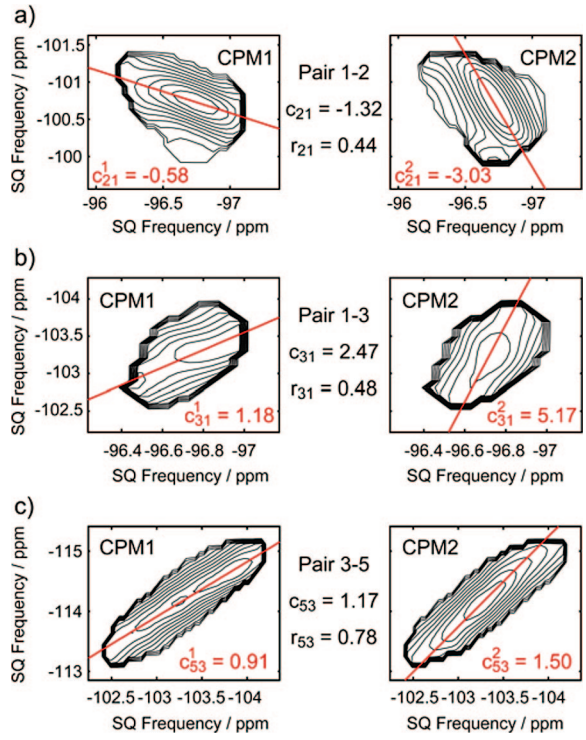

Figure 9. Examples of conditional probability matrices extracted from the 2D ^{29}Si{^{29}Si} zfr-INADEQUATE spectrum of Figure 8a, for the ^{29}Si−^{29}Si pairs 1−2 (a), 1−3 (b), and 3−5 (c). Superimposed in red are the best fits of CPM1 and CPM2 maximum intensities to straight lines, and the associated c^1_{ji} and c^2_{ji} values (with $i < j$). For each i−j pair, the calculated chemical shift correlation c_{ji} and the degree of correlation r_{ji} are indicated between the two conditional probability matrices.

$$r_{ji} = c_{ji}/\max(|c^1_{ji}|,|c^2_{ji}|) \qquad (11)$$

which ranges from zero to unity, with "zero" meaning there is no correlation and "unity" meaning that there is total correlation between the two sites. The results obtained for the different pairs of ^{29}Si sites are reported in the last two columns of Table 2, and different situations of two-site chemical shift correlation are illustrated in Figure 9. For example, pairs 1−2 (Figure 9a) and 1−3 (Figure 9b) illustrate the case of a rather low degree of correlation ($r_{ji} < 0.5$), which results in significantly different slopes c^1_{ji} and c^2_{ji}. In the case of pair 1−2, high frequencies are correlated with low frequencies of the other site ($c_{ji} < 0$), whereas pair 1−3 shows high frequencies correlated to high frequencies and low frequencies correlated to low frequencies, which corresponds to a positive correlation $c_{ji} > 0$. Finally, ^{29}Si−^{29}Si pair 3−5 (Figure 9c) illustrates the case of a high degree ($r_{ji} > 0.75$) of (positive) chemical shift correlation. In this material, because of the high degree of linearity of the observed cross-peaks and associated conditional probability distributions, the magnitude of the chemical shift correlation c_{ji} is directly related to the relative width of the 1D chemical shift distributions of sites i and j.[17] Moreover, it can be shown that the degree of correlation is also influenced to some extent by the width of the two correlating distributions. Indeed, when the peaks get narrower, the 2D chemical shift dispersion becomes smaller, and the effect of the limiting homogeneous broadening becomes larger, resulting in a loss of correlation. The implications of these parameters for the local disorder within the silicate framework are addressed below, in light of their relationship with the temperature dependence of the ^{29}Si peaks positions and broadenings.

4.c. Combined Analyses of the Static and the Temperature-Dependent Disorder. Quantitative cross-analyses of the site-to-site ^{29}Si{^{29}Si} chemical shift correlations at 298 K (Table 2) with the temperature dependences of the ^{29}Si chemical shifts (Figure 7a) provide important information on the nature of the disorder within the surfactant-templated silicate framework. For example, ^{29}Si sites 2 and 5 have an opposite temperature dependence (orange squares and blue crosses in Figure 7a), corresponding to chemical-shift-to-temperature slopes $a_2 = 0.014$ ppm/K and $a_5 = -0.020$ ppm/K with opposite signs, and thus a negative a_5/a_2 ratio of −1.5 (Table 2). The 2D correlation cross-peaks associated with this 2−5 ^{29}Si−^{29}Si pair (Figure 8a) have nearly perpendicular orientations, which is characteristic of a correlation between high frequencies of one site and the low frequencies of the other site.[17] The resulting chemical shift correlation c_{52}, obtained as described in section 4.b, is thus negative: $c_{52} = -2.0$. In contrast, the ^{29}Si peaks corresponding to sites 3 and 5 are both shifted to high frequencies when the temperature is decreased (red triangles and blue crosses in Figure 7a), resulting in a positive site-to-site temperature-dependence ratio $a_5/a_3 = 1.0$. In the case of this 3−5 pair, the static 2D ^{29}Si{^{29}Si} correlation line shapes at 298 K (Figure 8a) show remarkably parallel elongation (characteristic of a strong correlation between high frequencies of both sites, and between low frequencies of both sites, of similar 1D line widths[17]), with the associated site-to-site chemical shift correlation $c_{53} = 1.2$. These two examples suggest that, for a given ^{29}Si−^{29}Si pair i−j, the site-to-site temperature dependence ratio a_j/a_i and the site-to-site chemical shift correlation c_{ji} at a 298 K are most likely related. Indeed, Figure 7b shows a plot of the ^{29}Si{^{29}Si} chemical shift correlations at 298 K c_{ji} as a function of the temperature-dependence ratios a_j/a_i for all of the ^{29}Si−^{29}Si pairs of the surfactant-templated silicate framework. The "range" bars are delimited by the c^1_{ji} and c^2_{ji} site-to-site ^{29}Si{^{29}Si} chemical shift correlation slopes extracted from conditional probability matrices CPM1 and CPM2 (see section 4.b and Figure 8d or 9) and are directly related to $(r_{ji})^{-1}$ (eqs 10 and 11). They thus yield an indication of the degree of correlation; the smaller the "range" bar, the stronger the two-site chemical shift correlation. The correlation observed in Figure 7b between the site-to-site ratios of the temperature-dependent ^{29}Si chemical shifts (which are associated with a dynamic process), and the chemical shift correlations at 298 K (which correspond to static local structural disorder), is generally remarkable, close to a 1:1 correlation, as indicated by the solid line. This suggests that the static disorder within the silicate layers at ambient temperature and the disordering process that occurs when decreasing the temperature have a similar physicochemical origin.

The strong connection suggested by this observation between local framework disorder in the layered silicates and mobility of the surfactant species is further supported by detailed observation of the temperature dependence of each ^{29}Si MAS NMR peak (Figure 7a). Although they have been considered linear in the above analysis, the chemical shift variations are in fact more pronounced between 260 and 290 K (Figure 7a, gray-shaded region). This temperature range corresponds remarkably well to the critical-temperature regime observed for the line widths (see Figure 2b and section 3) and to the intermediate chemical-exchange regime of the surfactant headgroups discussed in section 3. Therefore, all of the information provided by the different analyses here (Figures 2b, 4b, 5b, and 7a) suggests that the static disorder at ambient temperature and the temperature-dependent shifts and broadening of the ^{29}Si NMR peaks arise from a single physical process, which appears to be

caused by (or at least is concomitant with) the freezing of the surfactant headgroup motions around 275 K.

One possible explanation for the broadening mechanism of the ^{29}Si MAS NMR peaks with decreasing temperature could thus be that reduction in the surfactant headgroup mobility induces a broader distribution of localized electrostatic or mechanical forces on the extremely thin (0.7 nm thick) silicate layers. The silicate framework might, as a result, experience increased local mechanical distortions, which would be associated with larger distributions of local geometries, such as Si−O−Si bond angles, and thus broader ^{29}Si chemical shift distributions.

However, a more plausible explanation is that slowing of the surfactant headgroup dynamics results in a static distribution of relative positions of the strongly interacting cationic surfactant headgroups with respect to the silicate layers *without otherwise distorting the silicate framework geometry*. As a consequence, a given ^{29}Si site in the silicate framework would experience a distribution of local interactions (e.g., electrostatic, hydrophilic, hydrophobic), which perturb the electronic density at the ^{29}Si sites, thus resulting in the observed broadening of the ^{29}Si MAS NMR peaks. The linear site-to-site correlations that are observed experimentally in Figures 8d and 9 and discussed in section 4.b suggest that each ^{29}Si site may be affected by a single parameter, such as its distance to the cationic surfactant headgroup(s). For translational disorder in one direction, for example along the *z*-axis perpendicular to the silicate layers, a monotonic dependence of the ^{29}Si chemical shifts of different ^{29}Si sites on their distances to the nearby alkylammonium headgroups would seem reasonable and would be consistent with the measured variations in the respective correlations.

This study provides a strong basis for a detailed understanding of the subtle temperature-dependent structural disorder observed in these materials, although further investigations are required to establish unambiguously the exact nature of the origin of the physicochemical process involved here. Analyses of similar samples with different compositions and prepared under different synthesis conditions can be expected to contribute to new molecular understanding of how order and disorder develop in this and other classes of templated organic−inorganic materials.

5. Conclusions

In summary, temperature-dependent ^{29}Si MAS NMR studies of short-range-ordered surfactant-templated layered silicate materials (prepared with 50% enrichment in ^{29}Si) show strong interrelationships between local framework ordering and disordering and the mobilities of the surfactant headgroups. On the basis of 2D ^{29}Si{^{29}Si} correlation NMR measurements, the effects of homogeneous and inhomogeneous broadening have been differentiated and analyzed. This allowed the quantitative characterization of the structure-directing surfactant headgroup motions at the silicate layer interfaces ($\Delta_r G^{\ddagger} = 58.8 \pm 0.3$ kJ·mol^{-1}) through ^{29}Si transverse dephasing time (T_2') measurements, as functions of temperature. To our knowledge, this is the first time that T_2' measurements have been used to probe dynamic processes in solids, and the simple model used here to describe the dynamics suffices to show the role of the surfactants in the disordering process of the silicate framework. A detailed cross-analysis of the temperature-dependent shifts and broadening of the ^{29}Si NMR lines strongly indicates that the static disorder of the silicate framework at ambient temperature arises from a single physicochemical process, which appears to be directly related to the freezing of the surfactant headgroup motions at their common interface. It is particularly interesting to note that the ^{29}Si nuclei register indirectly the dynamics of their nearby surfactant headgroups, to which they are sensitive through their ^{29}Si T_2' values. The ^{29}Si nuclei simultaneously and directly manifest the dynamically modulated and very subtle local disorder of the silicate framework through their chemical shifts and associated distributions. Because the dynamic and disordering processes can be observed at the same time and independently, they can be clearly distinguished. In the future, refined descriptions of the dynamics of the surfactants and nearby adsorbed solvent molecules may result from direct studies of the surfactants, and then be used to probe the robustness of our new approach that ascribes the origins of the disorder from the point of view of spectator nuclei to surfactant dynamics effects. Finally, further investigations are under way to discriminate between slight mechanical distortions of the silicate layers due to expansion/contraction of the surfactant domains and dispersion of the electrostatic environments at the layer interfaces, involving the cationic surfactant headgroups and solvent used for the synthesis of these fundamentally interesting and technologically important materials.

6. Experimental Section

6.a. Sample Preparation. The surfactant-templated layered silicates with molecularly ordered 1-nm-thick sheets were prepared with 50% ^{29}Si enrichment, as described previously.[14,15] The development of molecular order and resultant structures of the silicate layers are established by strong interactions between anionic silicate framework moieties and cationic headgroups of the $CH_3(CH_2)_{15}N^+(Me_2Et)$ surfactant molecules, which cannot be removed without the collapse and disordering of the layered silicate structure.

6.b. ^{29}Si NMR Experiments. All experiments were performed on a Bruker AVANCE-500 wide-bore NMR spectrometer operating at ^{1}H and ^{29}Si frequencies of 500.14 and 99.35 MHz, respectively. A 4 mm variable-temperature double-resonance magic-angle-spinning (MAS) NMR probehead was used with a MAS frequency of 10 kHz. Cross-polarization (CP) from ^{1}H to ^{29}Si was achieved with an adiabatic passage through the Hartmann−Hahn condition,[36] using a contact time of 8 ms. Heteronuclear decoupling was applied using the SPINAL64 decoupling scheme[37] with a proton nutation frequency of 100 kHz. Variable-temperature ^{29}Si CP MAS NMR experiments were conducted by sampling 8, 32, or 64 scans, depending on the spectral signal-to-noise ratio at a given temperature. Temperature calibration was performed using $Pb(NO_3)_2$, using the temperature dependence of the ^{207}Pb chemical shift (slope of 0.75 ppm/K).

Two-dimensional ^{29}Si{^{29}Si} *z*-filtered refocused (zfr) INADEQUATE NMR[19−21] spectra were acquired using ^{1}H adiabatic CP (circumventing the effects of the long longitudinal ^{29}Si spin relaxation times). An experimentally optimized (half) spin-echo delay (τ) of 8 ms was used for best overall efficiency. A *z*-filter of 30 ms (without heteronuclear decoupling) was applied to remove antiphase contributions to the spectra.[21] It has been shown[38] than no spin diffusion occurs under the above conditions on this type of sample. At 298 K, the indirect double-quantum (DQ) dimension was recorded with 160 t_1 increments using the TPPI procedure,[39] and 128 scans were summed for each increment using a recycle delay of 4.5 s. At 278 K, 192 scans were summed, and the recycle delay was 6 s.

Extraction of conditional probability matrices from 2D homonuclear correlation spectra was achieved by using a homemade Matlab routine that is available upon request from the authors.[17] This procedure has also recently been implemented in the matNMR toolbox of J. D. Van Beek.[40,41]

Transverse ^{29}Si dephasing times (T_2') were determined using a selective spin-echo ^{29}Si experiment. Semiselective soft pulses with Q3 Gaussian cascade[42] shape of 15 ms (Q^4 ^{29}Si sites 3, 4, and 5) or 20 ms (Q^3 ^{29}Si sites 1 and 2) were employed to refocus the desired ^{29}Si single-quantum coherences, while removing the J coupling modulations. Each experiment was conducted in a pseudo-2D manner, and the delay τ was incremented from 3 to 24 ms, with 32 or 64 transients summed, depending on the spectral signal-to-noise ratio. The T_2' values were determined by fitting the resulting integrated intensities, as a function of τ, to a monoexponential decay.

6.c. T_2' Error Calculations. The experimental errors of the NMR spectral integral intensities were estimated as the larger of either the spectral noise (one standard deviation) or twice the standard deviation of the fitted goal function. Monte Carlo error analyses were applied to estimate the errors of the determined transverse dephasing T_2' times. In these, a large number of similar fits were repeated with the addition of random noise (with a standard deviation equal to the experimental error bar) to the fitted points. The errors on the T_2' were then taken as the standard deviation of the series of T_2' values thus obtained.

Acknowledgment. Solid-state NMR spectra were recorded at the Rhône-Alpes Large Scale Facility for NMR (http://www.ralf-nmr.fr/). S.C. is grateful to the EGIDE and the French Minister of Foreign Affairs for providing him with a Lavoisier Fellowship 2006−2007 (File No. 487322K). The work at UCSB was supported in part by the U.S. Department of Energy, Office of Basic Energy Sciences, Catalysis Science Grant DE-FG02-03ER15467, and the UCSB Institute for Collaborative Biotechnologies. Finally, we are grateful to the referees for their helpful suggestions.

Supporting Information Available: Figure S1: post-C7 DQ ^{29}Si{^{29}Si} correlation spectrum of the layered silicate materials under study. This material is available free of charge via the Internet at http://pubs.acs.org.

References and Notes

(1) Corma, A. *Chem. Rev.* **1997**, *97*, 2373–2419.
(2) Stein, A. *Adv. Mater.* **2003**, *15*, 763–775.
(3) Yang, P. D.; Wirnsberger, G.; Huang, H. C.; Cordero, S. R.; McGehee, M. D.; Scott, B.; Deng, T.; Whitesides, G. M.; Chmelka, B. F.; Buratto, S. K.; Stucky, G. D. *Science* **2000**, *287*, 465–467.
(4) Schüth, F.; Schmidt, W. *Adv. Mater.* **2002**, *14*, 629–638.
(5) Soler-illia, G. J. D.; Sanchez, C.; Lebeau, B.; Patarin, J. *Chem. Rev.* **2002**, *102*, 4093–4138.
(6) Wan, Y.; Zhao, D. Y. *Chem. Rev.* **2007**, *107*, 2821–2860.
(7) Epping, J. D.; Chmelka, B. F. *Curr. Opin. Colloid Interface Sci.* **2006**, *11*, 81–117.
(8) Schmidt-Rohr, K.; Spiess, H. W. *Multi-dimensional solid-state NMR and polymers*; Academic Press: San Diego, 1994.
(9) Farnan, I.; Grandinetti, P. J.; Baltisberger, J. H.; Stebbins, J. F.; Werner, U.; Eastman, M. A.; Pines, A. *Nature* **1992**, *358*, 31–35.
(10) Stebbins, J. F.; Xu, Z. *Nature* **1997**, *390*, 60–62.
(11) Clark, T. M.; Grandinetti, P. J. *J. Phys.: Condens. Matter* **2003**, *15*, S2387−S2395.
(12) Youngman, R. E.; Haubrich, S. T.; Zwanziger, J. W.; Janicke, M. T.; Chmelka, B. F. *Science* **1995**, *269*, 1416–1420.
(13) De Paul, S. M.; Zwanziger, J. W.; Ulrich, R.; Wiesner, U.; Spiess, H. W. *J. Am. Chem. Soc.* **1999**, *121*, 5727–5736.
(14) Christiansen, S. C.; Zhao, D. Y.; Janicke, M. T.; Landry, C. C.; Stucky, G. D.; Chmelka, B. F. *J. Am. Chem. Soc.* **2001**, *123*, 4519–4529.
(15) Hedin, N.; Graf, R.; Christiansen, S. C.; Gervais, C.; Hayward, R. C.; Eckert, J.; Chmelka, B. F. *J. Am. Chem. Soc.* **2004**, *126*, 9425–9432.
(16) Sakellariou, D.; Brown, S. P.; Lesage, A.; Hediger, S.; Bardet, M.; Meriles, C. A.; Pines, A.; Emsley, L. *J. Am. Chem. Soc.* **2003**, *125*, 4376–4380.
(17) Cadars, S.; Lesage, A.; Emsley, L. *J. Am. Chem. Soc.* **2005**, *127*, 4466–4476.
(18) Wang, L. Q.; Exarhos, G. J. *J. Phys. Chem. B* **2003**, *107*, 443–450.
(19) Lesage, A.; Bardet, M.; Emsley, L. *J. Am. Chem. Soc.* **1999**, *121*, 10987–10993.
(20) Gunne, J. S. A.; Beck, J.; Hoffbauer, W.; Krieger-Beck, P. *Chem.—Eur. J.* **2005**, *11*, 4429–4440.
(21) Cadars, S.; Sein, J.; Duma, L.; Lesage, A.; Pham, T. N.; Baltisberger, J. H.; Brown, S. P.; Emsley, L. *J. Magn. Reson.* **2007**, *188*, 24–34.
(22) De Paepe, G.; Lesage, A.; Emsley, L. *J. Chem. Phys.* **2003**, *119*, 4833–4841.
(23) De Paepe, G.; Giraud, N.; Lesage, A.; Hodgkinson, P.; Bockmann, A.; Emsley, L. *J. Am. Chem. Soc.* **2003**, *125*, 13938–13939.
(24) De Paepe, G.; Lesage, A.; Steuernagel, S.; Emsley, L. *ChemPhys Chem* **2004**, *5*, 869–875.
(25) Vold, R. L.; Vold, R. R. *Prog. Nucl. Magn. Reson. Spectrosc.* **1978**, *12*, 79–133.
(26) Emsley, L.; Kowalewski, J.; Bodenhausen, G. *Appl. Magn. Reson.* **1990**, *1*, 139–147.
(27) Goldman, M. *Quantum Description of High Resolution NMR in Liquids*; Oxford University Press: Oxford, 1988.
(28) Palmer, A. G. *Chem. Rev.* **2004**, *104*, 3623–3640.
(29) Leigh, J. S. *J. Magn. Reson.* **1971**, *4*, 308–311.
(30) Eyring, H. *Chem. Rev.* **1935**, *17*, 65–77.
(31) Sandström, J. *Dynamic NMR Spectroscopy*; Academic Press: London, 1982.
(32) Martin, M. L.; Martin, G. J.; Delpuech, J.-J. *Practical NMR Spectroscopy*; Heiden, 1980.
(33) Harris, R. K. *Nuclear Magnetic Resonance Spectroscopy*; Longman: Harlow, 1986.
(34) Hohwy, M.; Jakobsen, H. J.; Eden, M.; Levitt, M. H.; Nielsen, N. C. *J. Chem. Phys.* **1998**, *108*, 2686–2694.
(35) Ernst, R. R.; Bodenhausen, G.; Wokaun, A. *Principles of Nuclear Magnetic Resonance in One and Two Dimensions*; Oxford Science Publications: New York, 1987.
(36) Hediger, S.; Meier, B. H.; Kurur, N. D.; Bodenhausen, G.; Ernst, R. R. *Chem. Phys. Lett.* **1994**, *223*, 283–288.
(37) Fung, B. M.; Khitrin, A. K.; Ermolaev, K. *J. Magn. Reson.* **2000**, *142*, 97–101.
(38) Cadars, S.; Lesage, A.; Hedin, N.; Chmelka, B. F.; Emsley, L. *J. Phys. Chem. B* **2006**, *110*, 16982–16991.
(39) Marion, D.; Wüthrich, K. *Biochem. Biophys. Res. Commun.* **1983**, *113*, 967–974.
(40) van Beek, J. D. *J. Magn. Reson.* **2007**, *187*, 19–26.
(41) Marcotte, I.; van Beek, J. D.; Meier, B. H. *Macromolecules* **2007**, *40*, 1995–2001.
(42) Emsley, L.; Bodenhausen, G. *J. Magn. Reson.* **1992**, *97*, 135–148.
(43) The Arrhenius rate law is also commonly used in NMR, but this equation contains an additional unknown parameter, the so-called preexponential factor, which introduces additional uncertainty in the context of the present analyses.
(44) This assumption is reasonable, because decoupling is expected to be more difficult at low temperatures, where the dynamics slow and the material becomes more solid-like.
(45) Errors were calculated using a Monte Carlo approach, moving each fitted point randomly within a Gaussian distribution of standard deviation equal to the associated error bar. The error reported corresponds to the standard distribution of the fitted values, over 1024 steps.
(46) An alternate possibility is that a three-site or higher-order exchange process could be considered, instead of the simple two-site exchange used here. However, such a model would involve additional variables that would increase the uncertainty of the analysis. It is not obvious that adding extra sites would substantially affect the results or conclusions.

JP711398H